Journal of Applied Fluid Mechanics, Vol. 10, No. 1, pp. 169-182, 2017.
Available online at www.jafmonline.net, ISSN 1735-3572, EISSN 1735-3645.
DOI: 10.18869/acadpub.jafm.73.238.26556

Heat Transfer Enhancement in a Stagnant Dielectric Liquid by the Up and Down Motion of Conductive Particles Induced by Coulomb Forces

G. Eslami[1], E. Esmaeilzadeh[1†], P. García-Sánchez[2], A. Behzadmehr[3] and S. Baheri[1]

[1]*Department of Mechanical Engineering, University of Tabriz, Tabriz, Iran*
[2]*Departamento de Electrónica y Electromagnetismo, Facultad de Física, Avenida Reina Mercedes s/n, 41012 Sevilla, Spain*
[3]*Department of Mechanical Engineering, University of Sistan and Baluchestan, P.O. Box 98164-161, Zahedan, Iran*

†*Corresponding Author Email: esmzadeh@tabrizu.ac.ir*

(Received May 16, 2016; accepted September 7, 2016)

ABSTRACT

When charged particles are exposed to an electric field the well-known Coulomb force acts on them. In this investigation, this force is utilized to induce vertical motion of spherical steel particles submerged in a dielectric liquid. The interelectrode space of a two parallel electrode system is filled with the liquid and dispersed steel particles, which become charged after contact with the electrodes. Experiments were carried out to measure the effect of this particle motion on the heat transfer between an electrode surface and an adjacent stagnant dielectric liquid. In order to interpret the experimental data, the dynamics of particles was analytically studied for low particle volume concentrations. Experimental results demonstrate significant heat transfer enhancement on low viscosity dielectric liquids. A detailed discussion is presented on the possible mechanisms responsible for such an enhancement.

Keywords: Heat transfer enhancement; Particle motion; Coulomb forces; Dielectric liquid.

1. INTRODUCTION

Tiny solid particles dispersed in a liquid or gas flow can influence the heat transfer process in a medium by various mechanisms. One of the effective mechanisms is the mixing (or stirring) action that is induced in the surrounding medium by the motion of particles in the bulk of the medium. Another mechanism arises from the particle-wall interactions where bombarding of the wall by particles causes a thinning of the viscous boundary sub-layer (Özbelge, 2001). In two-phase flows of moderate to high particle volume concentration, the particle-turbulence interaction mechanism also holds a great importance (Arcen *et al.*, 2012). Furthermore, the total heat capacity of the solid-liquid two phase medium is another factor that can affect the heat transfer rate. All these factors can reduce the heat resistance of the medium and, subsequently, aids to the transport of thermal energy. A theoretical study about different mechanisms of local heat transfer enhancement raised by bombardment of a surface by spherical particles can be found in Murray (1994a). Indeed, adding micron-sized solid particles into the fluid flow is a common strategy for heat transfer augmentation, and many technical notes and papers are available about this technique under the title of "particulate flow" or "fluidized bed" (Feng and Michaelides, 2009; Dan and Wachs, 2010; Nirmala and Muruganandam, 2015). Several external agents have been used by researchers for deriving and controlling the dispersed phase in the suspensions. Not all but a few are magnetic fields (Rawat *et al.*, 2014), sound waves (Wankhede *et al.*, 2011; Xu *et al.*, 2006), container vibration (Bacelos *et al.*, 2011) and mechanical stimulation (Siebert *et al.*, 1999). The mentioned technique is often difficult to be implemented in practice due to a substantial problem of sedimentation of the dispersed micron-sized particles in the flow. However, the main idea of adding solid particles into a flow as a heat transfer enhancement method still works (Flamant *et al.*, 2014). For an instance, a nanofluid which is an effective medium for heat transport, contains nanosized solid particles suspended in a base liquid. In fact, reducing the size of particles from the micrometer to the nanometer scale decreases the sedimentation rate considerably

and significantly improves the stability of the medium via inter-molecular forces (of course, the mechanisms of heat transfer in nanofluids are different from those discussed here). In addition to the reduction of particle size, another beneficial way to tackle the problem of particle sedimentation is forcing the submerged particles to move continuously in the liquid in order to prevent them from sedimentation. This task can be fulfilled by electric fields. An electric field can give rise to Coulomb force that acts on the particles against gravitational force. This method is known as electrostatic fluidization in the literature studied, for instance, by Bologa and Berkov in 1987 and Zhebelev in 1991.

In this paper we discuss the use of electric fields as an external agent to force the solid particles to move in a stationary viscous medium. To this end, we exploit the well-known motion of a conductive particle between two flat parallel metal plates under the influence of an electric field (Choi *et al.,* 2001; Asano *et al.,* 2002). Indeed, a single conductive particle becomes charged through induction when placed on an electrode and, for a sufficiently high voltage difference between the plates, the particle lifts off the electrode and moves towards the other electrode. Different dynamic behaviors can appear depending on the strength of the external electric field, size and density of the particle and viscous medium properties. As there are various industrial situations involving conductive particles subjected to electric fields, several investigations have been carried out in this regard. Choi *et al.* (2000) studied experimentally the motion of a single glassy carbon spherical particle in silicon oil under the uniform electric field between parallel plate electrodes. Asano *et al.* (2002) conducted some careful experiments with millimeter sized glassy carbon and steel spheres in the parallel electrode system. They observed the peculiar behavior in which conductive particles stay on the electrodes for a while after collision. An interesting application of two parallel electrodes system was recently introduced by Kawamoto (2009). He utilized this system in order to manipulate a single conductive or insulating fine particles with DC electric field. Recently Drews *et al.* (2014) used a Stokesian dynamic-like approach for computing the charge and force on a conducting spherical particle between two parallel electrodes.

Although the dynamic behavior of conductive particles in a medium containing dielectric gas or liquid under an electric field is widely investigated by a large number of researchers, it is difficult to find a study in the literature dealing with the heat transportation caused by such particle movements (Bologa *et al.,* 1985). This is the main objective of the present work. Effectiveness of the proposed method will be revealed by comparison of the magnitude of heat transfer rate between two cases "with" and "without" utilizing electric fields for fluidization of spherical particles submerged in a viscous dielectric medium. Another goal is gathering experimental data for evaluating future numerical studies. To the best knowledge of the authors, there is no experimental study on a case similar to our configuration and circumstances.

2. EXPERIMENTAL SETUP AND DATA REDUCTION

Our objective is to study the effect of the particle motion and collision with a heat transfer surface (HTS) on the heat transfer rate between that surface and the surrounding viscous medium. Figure 1 shows a schematic representation of the experimental setup. The main part of the setup is a rectangular container made of special plexi-glass (1) with side walls 10 mm thick. (Underlined numbers in the text of this section refer to the corresponding ones shown in Fig. 1). Two small holes drilled on the container's wall serve as liquid inlet and air outlet. The container is completely transparent to allow for observation of the particles motion of the particles (2) submerged in the dielectric liquid (3). Also, it is sufficiently resilient against high voltage electric potential. A copper flat plate (4) 100 mm long, 50 mm wide and 2 mm thick was attached on the floor of the container and connected to a high voltage supplier (5) with positive polarity. Another copper plate (6) with the same dimensions (100 mm × 50 mm × 2 mm) was placed on top of the container and connected to ground. A photograph of the test section is given in Fig. 2. The interelectrode distance is adjustable through the screw shown in Fig. 2. When the voltage supplier is switched on, a uniform electric field is set in the interelectrode space. The electric field induces the vertical motion of the conductive particles across the interelectrode gap. The electric current across the interelectrode gap is recorded by a pico-ammeter (7) connected in series with the high voltage supplier. The pico-ammeter was shield against any capacitive discharge by a resistor with a high electric resistance. The upper plate (grounded electrode), plays the role of a heat transfer surface (HTS) with a constant temperature of T_{ue}. T_{ue} is maintained constant by using a water flow (8) produced by a constant temperature bath (9). During each experiment, the value of T_{ue}, was available at any moment by reading the signal of a thermocouple (10) mounted on the center of the upper electrode. Maximum deviation of T_{ue}, from the desired constant value was less than $1C^{\circ}$ in all tests. The heating energy gradually transfers from the hot upper electrode to the cold liquid inside the container during each test. The magnitude of transferred heat from the upper electrode to the two phase medium can be estimated as:

$$Q_{\varphi}(t) = m_f c_M \left[\overline{T}_M(t) - T_0 \right] \tag{1}$$

where m_f is mass of the fluid, c_M, T_0 and $\overline{T}_M(t)$ are the specific heat capacity, the initial temperature and the mean temperature of the solid-liquid two phase medium, respectively.

$$c_M = c_f + \varphi c_p, \tag{2}$$

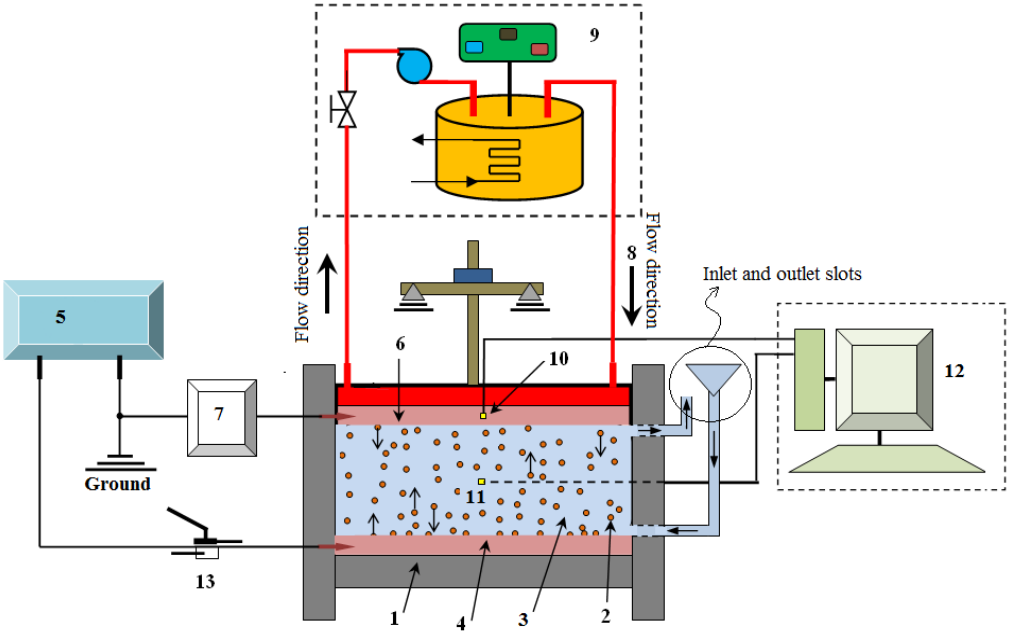

Fig. 1. Schematic representation of the experimental set-up; Plexi-glass container (1), conductive particles (2), dielectric liquid (3), High voltage electrode (4), High voltage supplier (5), Grounded electrode (6), Pico-ammeter (7), Constant temperature flow (8), Constant temperature bath (9), Thermocouples (10 and 11), Data acquisition unit (12), High voltage on-off switch (13).

in which φ denotes the mass loading ratio;

$$\varphi = \frac{m_p}{m_f}. \tag{3}$$

where m_p is total mass of particles dispersed in the working fluid.

When there is no particle in the medium and no potential difference between the two electrodes (i. e. $\varphi = 0,\ \Delta V = 0$), the total heat transferred from the

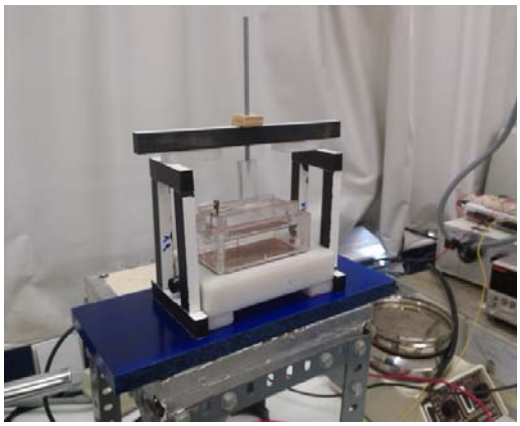

Fig. 2. Photograph of the test section.

HTS to the liquid is (see Eq. (1)):

$$Q_0(t) = m_f c_f \left[\overline{T}_f(t) - T_0\right] \tag{4}$$

in which

$$\overline{T}_f(t) = \overline{T}_M(t)\big|_{\varphi=0} \tag{5}$$

The ratio of $\eta = Q_\varphi(t)/Q_0(t)$ is a reasonable indicator of the effectiveness of the implemented technique for enhancing the heat transfer rate in the configuration under study. Considering Eqs. (1), (2) and (4):

$$\eta = \left[1 + \varphi \frac{c_p}{c_f}\right] \frac{\overline{T}_M(t) - T_0}{\overline{T}_f(t) - T_0}. \tag{6}$$

We define the heat transfer enhancement factor (*HTEF*) as:

$$HTEF = \eta - 1 \approx \left[1 + \varphi \frac{c_p}{c_f}\right] \frac{T_{C,M}(t) - T_0}{T_{C,f}(t) - T_0} - 1, \tag{7}$$

where $T_{C,f}(t) = T_{C,M}(t)\big|_{\varphi=0}$, and $T_{C,M}(t)$, is the temperature of the medium central point which was considered as an approximation to the medium mean temperature, $\overline{T}_M(t)$.

$T_{C,M}(t)$, was measured by another thermocouple (11) and recorded during each experiment via a data acquisition unit (12). It should be noted that, in order to protect the thermocouple from the effects of intensive electric field, a suitable protocol should be adopted for measuring $T_{C,M}(t)$. For this purpose, the voltage supplier is turned off by a high voltage switch (13) prior to the measurement of $T_{C,M}$.

3. MATERIALS AND METHODS

Spherical particles made of steel were used as conductive particles (Lianyungang Dongkun Inductry and Trade Co., Ltd.). Silicon oil and Opticool (class H) (DSI Ventures, Inc.) were utilized throughout the present study as dielectric liquids. Opticool Fluid is an isoparaffin-based, non-toxic, colorless and odorless dielectric heat transfer fluid. A very low viscosity and a fairly high thermal conductivity make it an ideal candidate for removing heat from circuitry with high heat flux densities. It is usually preferred for cooling equipment involving high-volage technologies. Some properties of the utilized particles and liquids are given in the Table 1. Throughout all experiments, around 6000 equally-sized steel balls of $0.3mm$ diameter were dispersed in 0.1 liter of the working dielectric liquid. Experiments were carried out with either silicon oil or opticool as the working fluid and the applied potential difference to the electrodes was in the range $7kV \le V \le 19kV$. Based on Eq. (3), the mass loading ratio was $\varphi = 0.697\%$ for the experiments with silicon oil, and $\varphi = 0.805\%$ in the case of opticool. For each experiment, the uniform electric field and the subsequent up and down motion of particles was carefully established for 5 minutes ($t_{end} = 5\,min \pm 5\,sec$).

Table 1 Test particles and liquids properties

Particle properties		
Material	Steel	
Diameter, $D\ (mm)$	0.3	
Density, $\rho_p\ (kg/m^3)$	7830	
Heat capacity, $c_p\ (J/kg.K)$	464	
Conductivity, $k_p\ (W/m.K)$	54	
Liquid properties		
Material	Opticool	Silicone oil (20Cs)
Viscosity, $\mu\ (Pa.s)$	0.0021	0.019
Density, $\rho_f\ (kg/m^3)$	825	953
Heat capacity, $c_f\ (J/kg.K)$	2300	1500
Conductivity, $k_f\ (W/m.K)$	0.135	0.14
Charge relaxation time, $\tau_c\ (sec)$	15.4	17.1

Three series of experiments were conducted: A, B and C. Silicon oil was used as the working fluid for the tests of series A. Experiments of series B were performed with the same conditions of series A but using Opticool as the working liquid. Throughout experiments of both series A and B, initial temperature difference between the liquid and the upper electrode surface was set to $\Delta T_i = 40 \pm 1\ ^\circ C$ and the interelectrode distance was adjusted to $d = 20\ mm$. Experiments of series C were performed in order to investigate the effect of ΔT_i on the heat transfer process.

An analysis of the errors of experimental data was based on Beckwith *et al.* (2007) and maximum uncertainty of 5.45% was predicted for *HTEF* (see appendix for more details). Reproducibility of the tests was assessed and confirmed by repetition under identical experimental conditions.

Note that in the present tests, the particle volume concentration is:

$$\frac{N_p \pi D^3/6}{V_{liquid}} \times 100 = \frac{6000 \times \pi (0.3mm)^3/6}{100 \times 50 \times 20 mm^3} \times 100 = 0.085\%,$$

which is sufficiently small to guarantee the validity of the assumption of negligible hydrodynamic and electrical interaction between particles. It is worth to point out that in a similar experiment on the fluidization of electrically conductive particles (bronze spheres with density of 8840 kg/m3 and mean diameter of 0.286 mm), Bologa and Berkof (1987), demonstrated that for a volume concentration below 0.11%, the effect of particles on each other motion is negligible.

4. JOULE HEATING EFFECT

In addition to the upper electrode, the so called Joule heating effect is a source of heat for the particle-liquid dispersion. The magnitude of this effect is estimated by the following formula:

$$Q_J(t) = \int_0^{t_{end}} \Delta V\ I(t)dt, \tag{8}$$

where ΔV is the electric potential difference between the two electrodes and $I(t)$ is the electric current passing through the dispersion (i.e. the current recorded by the picometer (7)). Since both working liquids are strong dielectrics, the electric current is often in the nano-ampere range. However, the presence of conductive tiny particles in the liquid increases the electric current $I(t)$ considerably. Throughout this study, a maximum average electric current of $\bar{I} \approx 1.5\mu A$ was measured for an electric potential difference of $\Delta V = 19kV$ and time interval of $\Delta t = 5$ minutes. Substitution of these values in the Eq. (8) gives $Q_J = 8.6\,J$. The increase in average temperature of the mixture caused by this thermal energy is below $0.05^\circ C.$, negligible in comparison with the increment caused by the upper hot electrode (several degrees). Thus, the Joule heating effect is ignored in this study.

5. PARTICLE DYNAMICS

In order to interpret the results of the heat transfer tests, it is essential to understand the effect of various pertaining parameters on the particle dynamics, particularly, on the particle velocity and Reynolds number. As previously mentioned, the volume concentration of dispersed particles in the current study is very low and no considerable hydrodynamic or electrical interaction exists between particles. Based on the experiments, two different kind of dynamic behavior are generally observed for a particle located on the lower electrode surface. In one case, the particle cannot reach the upper electrode after detaching from the lower due to charge leakage from the particle surface to the surrounding fluid. Thus, the particle falls down due to gravitational force and contacts with the lower electrode, repeating the motion. In the second scenario, the particle rises until it reaches the upper electrode. As the particle approaches that electrode, the electric field between the particle and the electrode increases and, eventually, a micro-discharge would occur between them (Dascalescu *et al.,* 1998). During the micro-discharge, the particle exchanges some electric charge with the electrode, delivering part of the charge which had been obtained from the far electrode and gaining countercharge from the close electrode. Then, it repels from the close electrode moves back to the lower electrode. This scenario will hold as long as the electric potential difference between the two electrodes is maintained. Depending on the charge relaxation time of the medium (τ_c), one or the other scenario will take place. When τ_c is large in comparison with the particle flight time τ_{flight}, the second scenario appears (i.e. $\tau_c/\tau_{flight} \gg 1$). Based on our direct experimental observations, we will consider this scenario in the following analysis of particle dynamics.

5.1 Equation of Motion

Ignoring the history force (Brennen, 2005), the electrical image forces (Perez, 2002) and the so called wall effect on the hydrodynamic forces (Ardekani and Rangel, 2008) as well as assuming a large charge relaxation time for the surrounding liquid (second scenario), a simplified equation governing the upward motion velocity, $u_1(t)$ and the downward motion velocity, $u_2(t)$ of a single particle, can be written as:

$$(M_p+\frac{1}{2}M_f)\frac{d}{dt}\begin{bmatrix}u_1(t)\\u_2(t)\end{bmatrix}=\begin{bmatrix}1\\-1\end{bmatrix}E_0 q_p-(M_p-M_f)g+\frac{1}{2}\rho_f\begin{bmatrix}-u_1^2\\u_2^2\end{bmatrix}C_D\frac{\pi D^2}{4} \quad (9)$$

where, $E_0 = V/d$ is the uniform electric field strength with V and d being the electrical potential of the powered electrode and the interelectrode distance, respectively. q_p stands for the charge transferred to the particle surface after colliding with the electrodes. C_D is the drag coefficient, which can be calculated, for example, by the following formula of Clift *et al.,* (1978) used in many studies in the range $1 < Re < 800$.

$$C_D = \frac{24}{Re}(1+0.15\,Re^{0.687}) \quad (10)$$

The particle charge can be obtained using the well-known Flechi formula (Dascalescu, 1998) which is used for a conductive spherical particle placed on an electrode and exposed to uniform electric field E_0;

$$q_p = \frac{\pi^2}{6}\pi D^2 \varepsilon E_0 \quad (11)$$

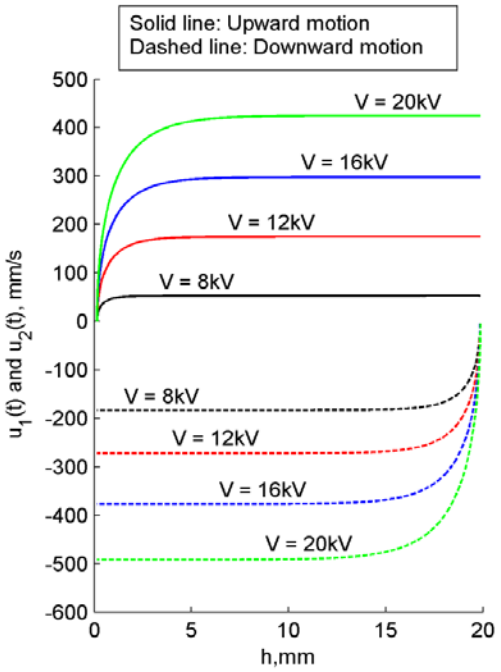

Fig. 3. Instantaneous velocity of a single steel particle with 0.3 mm diameter moving inside opticool in the interelectrode space. Depicted results were derived by numerical solution of Eqs. (9-11). See Table 1 for numerical values of other parameters.

Equation (9) was numerically solved using Eqs. (10) and (11), with initial condition $u(0) = 0$, for obtaining the particle instantaneous velocity. Figure 3 shows $u_1(t)$ and $u_2(t)$ versus the distance of the particle center to the lower electrode for different values of the powered electrode voltage. It can be observed that, for any value of the applied voltage, the particle reaches the terminal velocity rapidly after detaching from the electrodes. Thus, terminal velocities $u_{\infty 1}$ and $u_{\infty 2}$ would be considered as typical velocity scales for estimating the effect of the particle dynamics on the heat transfer

enhancement. Note that, because the wall effects (Izard *et al*. 2014) are neglected, the otherwise expected sharp reduction in particle velocity is not observed in the regions close to the electrodes. Further discussion is available at the section 8

5.2 Analytical Formula for the Particle Terminal Velocities

Although the drag coefficient given by Eq. (10) is useful for the numerical computations, it is not suitable for obtaining a simple analytical formula to calculate the terminal velocities $u_{\infty 1}$ and $u_{\infty 2}$ and, consequently, $Re_{\infty 1}$ and $Re_{\infty 2}$. This issue can be alleviated for low Reynolds numbers by using the following relation (Eq. 12) for the drag coefficient. It is derived by fitting a curve for data calculated from Eq. (10) in the range $1 < Re < 100$ with the coefficient of determination $R^2 = 0.9997$.

$$C_D = a + \frac{b}{Re} + \frac{c}{Re^2} \tag{12}$$

where $a = 0.936$, $b = 30.33$ and $c = -2.284$.

By substitution of $du_1/dt = 0$, $u_1 = \mu Re_{\infty 1}/\rho_f D$ and $M_p = \rho_p \pi D^3/6$, $M_f = \rho_f \pi D^3/6$ in to the Eq. (9) and using Eq. (11) and (12) respectively for the drag coefficient and the particle charge, we have:

$$aRe_{\infty 1}^2 + bRe_{\infty 1} + c = \frac{4}{3}\frac{\rho_f}{\mu^2} D^2 \left[\pi^2 \varepsilon E_0^2 - (\rho_p - \rho_f) gD\right] \tag{13}$$

where $Re_{\infty 1}$, denotes the particle terminal Reynolds number during its upward motion. $Re_{\infty 1}$ can be obtained simply by solving the above algebraic equation.

In a similar way, for the downward motion of a single particle, Eq. (9) is reduced to:

$$aRe_{\infty 2}^2 + bRe_{\infty 2} + c = \frac{4}{3}\frac{\rho_f}{\mu^2} D^2 \left[\pi^2 \varepsilon E_0^2 + (\rho_p - \rho_f) gD\right]. \tag{14}$$

where $Re_{\infty 2}$, denotes the particle terminal Reynolds number during its downward motion. Comparison between Eqs. (13) and (14) shows that the dynamic behavior of a typical single particle during its upward motion can be very different from that of downward motion depending on the particle to liquid density ratio. The larger the density ratio, the greater the difference. Typical roots of Eqs. (13) and (14) are depicted in Fig. 4 for steel particles of different size submerged in the opticool liquid and affected by an electric field of strength $E_0 = 0.55\ MVm^{-1}$. It is worth to note that, while the downward terminal Reynolds number $Re_{\infty 2}$ increases with the particle diameter, the upward Reynolds number $Re_{\infty 1}$ is non-monotonous. An optimum particle diameter corresponding to the maximum terminal Reynolds number can be determined by imposing $d\,Re_{\infty 1}/dD = 0$ in Eq. (13) as:

$$D_{opt} = \frac{2\pi^2}{3}\frac{\varepsilon E_0^2}{(\rho_p - \rho_f) g}\ . \tag{15}$$

In Fig. 4 the optimum diameter is $D_{opt} = 570\mu m$ which gives a maximum particle terminal Reynolds number $Re_{\infty 1,\max} = 27.5$.

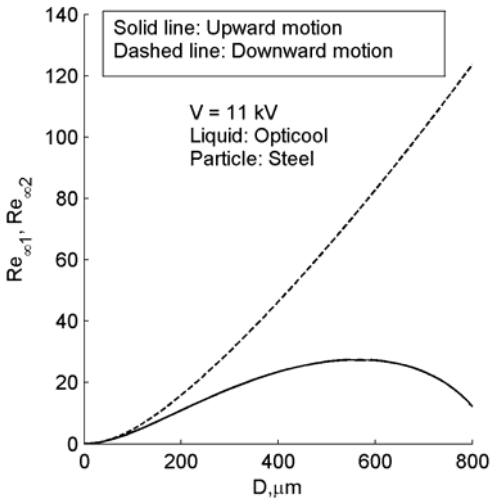

Fig. 4. The particle terminal Reynolds number during upward and downward motion as a function of the particle diameter. Results obtained for steel particles submerged in opticool liquid and subjected to; $V = 11kV$, $d = 20mm$.

5.3 Particle Terminal Reynolds Numbers in the Present Experiments

Figure 5 shows solutions of algebraic Eq. (13) and (14) for the conditions of the present experiments. That is a steel particle of $300\mu m$ diameter immersed in either silicon oil or opticool liquids and, subjected to electric fields of different strengths. It can be seen that the particle terminal Reynolds number scales linearly with voltage within the studied range. Also, the terminal Reynolds number for the particle moving in silicon oil is considerably lower than that for opticool. Furthermore, the upward and downward motion in silicon oil takes place with approximately the same terminal Reynolds number (in contrast to opticool). These differences, as well as other observable tendencies in Fig. 5, are caused by a large difference between viscosities of the two liquid. The model predicts $0.6 \le Re_{\infty 1,2} \le 2.4$ and $2.1 \le Re_{\infty 1,2} \le 57$ for the particles submerged in silicon oil and opticool, respectively.

It is essential to note that the aforementioned analysis assumes large values of τ_c. However, many factors including small amounts of chemical impurity and water content can dramatically reduce the charge relaxation time of the dielectric liquid (Park *et al.,* 2014; Schober *et al.,* 2009). Reduction of τ_c would significantly change the scenario.

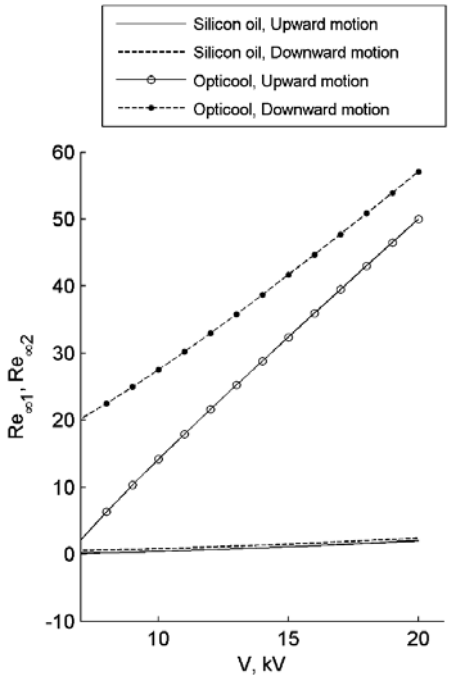

Fig. 5. Terminal Reynolds number of a single test particle ($Re_{\infty 1}$ and $Re_{\infty 2}$) for the conditions of the present experiments. (a steel particle with $D = 0.3mm$)

6. VALIDATION BY NUMERICAL SIMULATION FOR THE CASE OF NO DISPERSED PARTICLES

An exact numerical solution of the current problem requires a direct numerical solution (DNS) technique such as arbitrary Lagrangian–Eulerian method (ALE) (Gan *et al.,* 2003) or Distributed Lagrange Multiplier/Fictitious Domain method (DLM/FD) (Dan and Wachs, 2010). Such simulations for the current problem are very complicated particularly due to the electric field effects. They are also very time consuming and memory demanding because of large number of the spherical particles dispersed in the medium. Therefore, such simulations are beyond the present work. However, in a special case, without the presence of moving particles inside liquid, the heat transfer procedure can be straightforwardly simulated. Although this is only a special case and does not include the main phenomenon of the vertical motion of dispersed particles, it is still useful because it can evaluate the medium's central point temperature, $T_{C,f}(t)$, which is used for calculation of *HTEF* according to Eq. (7).

In this special case, neither free nor forced convection takes place inside the liquid domain. Because the liquid is at rest and the hotter plate locates above the liquid, the only relevant heat transfer mechanism is conduction through which the heat is transferred from the upper electrode to the adjacent stagnant liquid and to the plexi-glass container body.

Governing equations and appropriate boundary and initial conditions are:

- For the liquid domain:

$$\begin{aligned} &\frac{\partial^2 T_1}{\partial x^2}+\frac{\partial^2 T_1}{\partial y^2}+\frac{\partial^2 T_1}{\partial z^2}=\frac{1}{\alpha_f}\frac{\partial T_1}{\partial t},\\ &T_1\big|_{t=0}=T_0,\\ &\left.\frac{\partial T_1}{\partial z}\right|_{lower\ electrode\ (z=0)}=0,\\ &T_1\big|_{upper\ electrode\ (z=H)}=T_{up}. \end{aligned} \tag{16}$$

- For the plexi-glass container:

$$\begin{aligned} &\frac{\partial^2 T_2}{\partial x^2}+\frac{\partial^2 T_2}{\partial y^2}+\frac{\partial^2 T_2}{\partial z^2}=\frac{1}{\alpha_2}\frac{\partial T_2}{\partial t},\\ &T_2\big|_{t=0}=T_0,\\ &\left.\frac{\partial T_2}{\partial z}\right|_{z=0\ \&\ z=H}=0,\\ &k_2\left.\frac{\partial T_2}{\partial n}\right|_{outer\ vertical\ surfaces}=\bar{h}_V\left(T_2(t)-T_\infty\right), \end{aligned} \tag{17}$$

Boundary conditions for the liquid-container interface read:

$$\begin{aligned} &T_1\big|_{interfaces}=T_2\big|_{interfaces},\\ &k_f\left.\frac{\partial T_1}{\partial x}\right|_{interfaces}=k_2\left.\frac{\partial T_2}{\partial x}\right|_{interfaces},\\ &k_f\left.\frac{\partial T_1}{\partial y}\right|_{interfaces}=k_2\left.\frac{\partial T_2}{\partial y}\right|_{interfaces}. \end{aligned} \tag{18}$$

where $T_1=T_1(x,y,z,t)$ and $T_2=T_2(x,y,z,t)$ denote the temperature distribution in the liquid and the container medium, respectively. T_0 is the initial temperature of the solution domains (liquid and its container). T_{up} refers to the upper electrode constant temperature. α_2 and k_2 are thermal diffusion and heat conductivity of plexi-glass, respectively. $\bar{h}_V$ means the surface-averaged convective heat transfer for the natural convection between the environment and vertical lateral surfaces of the container.

In this simulation we considered $\bar{h}_V \approx 6$ which was calculated based on the following formula (David, 2012).

$$\overline{Nu}_V = 0.68+\frac{0.67Ra_V^{0.25}}{\left[1+(0.492/\mathrm{Pr})^{9/16}\right]^{4/9}} \tag{19}$$

A finite element method was used for solving the governing Eq. (16), (17) and (18).

Temperature distribution in the mid-planes of the solution domains for $t=5\,\mathrm{min}$ has been shown in Figs. 6(a) and (b). As seen in both figures and as expected, the heat is diffused from the upper electrode into the liquid one-dimensionally (-z-coordinate direction) and very uniform temperature distribution is observed in the horizontal planes

except in a thin layer close to the container walls. It is worth to note that the temperature of the container's outer surface is still low after 5 minutes. Hence, the natural convection, as mentioned, does not significantly influence the results.

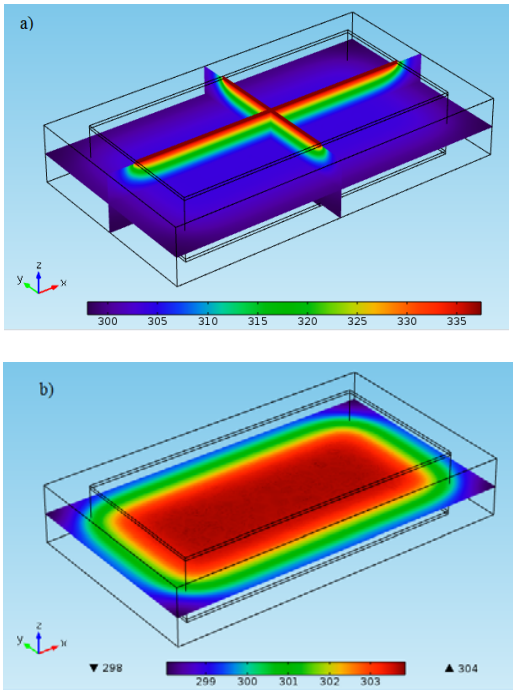

Fig. 6. Temperature distribution in the mid-planes for $t = 5 \times 60\,\text{sec}$, a) three plans are presented by $x = 60mm$, $y = 35mm$ and $z = 10mm$ b) plane of $z = 10mm$.

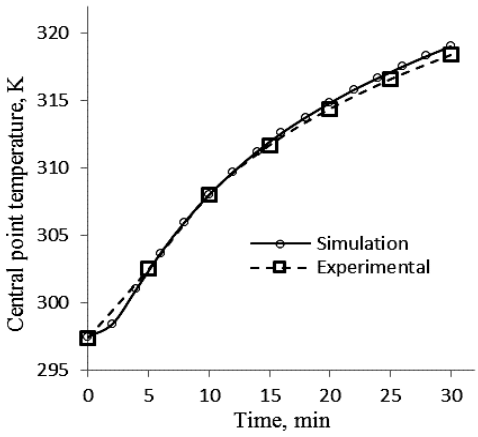

Fig. 7. Temporal evolution of the temperature in the central point of the liquid volume. Comparison between simulation results and measured data.

Figure 6 (a) indicates that temperature of the upper electrode and its adjacent layer of stationary liquid are close to each other. This augments thermal resistance and consequently reduces the heat transfer rate from HTS to the liquid. We believe that the up and down motion of particles can displace and stir the liquid layers close to the HTS and decrease accordingly the thermal resistance. This subject is described in detail in the section 8.

In Fig. 7 the simulation result for the temporal evolution of the domain's central point is compared with the corresponding measured data. As seen, very good agreement exists between them in the interval of 30 minutes, which validates the implemented devices and measurement techniques.

7. EFFECTIVE MECHANISMS

Before examining the details of the experimental results, it is convenient to discuss the various mechanisms through which the motion of particles influences the heat transfer rate in the configuration under study. The effect of moving particles on transportation of heat from an impingement surface (here the upper electrode) to the adjacent liquid can be participated to the following three distinct mechanisms.

- Bombardment mechanism (BM)
- Mixing mechanism (MM)
- Particle rebound mechanism (PRM)

7.1 Bombardment Mechanism (BM)

The bombardment mechanism relates to the bombardment of the heat transfer surface (HTS) by impinging particles. This mechanism acts by squeezing the liquid out from the particle-HTS gap via impinging particles which consequently results in creation of convective heat transfer between the HTS and adjacent liquid. A typical squeezing flow of a Newtonian and Non-Newtonian fluid between an approaching spherical particle and a plane wall has been studied by Despeyroux and Anbari (2012). From the velocity field in the particle-wall gap (see Fig. 2 in Despeyroux and Anbari (2012)), it can deduce that a significant heat transfer can occur by transient forced convection mechanism whenever a temperature difference exists between the particle and the interstitial fluid. Also, the heat transfer in the squeezing flow between two flat surfaces has been widely studied (Khaled and Vafai, 2004, 2005) which almost unanimously confirm heat transfer augmentation.

For a particular particle and a given interval of time, the particle impinging velocity, u_{imp}, and number of collisions between the particle and the HTS, N_c, are two functional factors which determine how much the BM is effective in enhancing of the heat transfer. Obviously, larger u_{imp} and N_c will result in more effectiveness of this mechanism.

7.2 Mixing Mechanism (MM)

The Mixing mechanism, in contrast to the bombardment one, acts on the bulk of the liquid. It refers to the reduction of temperature gradients in the heat transfer direction through mixing in the

bulk of the liquid. Indeed, when the particles vertically move inside the liquid, they disturb various layers of the stationary liquid and displace the liquid in short distances. Such liquid displacement brings about a convection-like effect in the medium which augments the heat transfer rate and increase the stored thermal energy. Relation between characteristics of a particle motion and the consequent mixing effect in its surrounding medium has not been clearly formulated. However, at a first glance, it can be said that magnitude of the liquid displaced by the particle motion and wake structure behind the moving particle are two dominant factors. Generally, as Hetsroni *et al.* (2001) has shown, the region behind an obstacle is very interesting in view of the heat transfer enhancement.

7.3 Particle Rebound Mechanism (PRM)

The particle rebound mechanism (PRM) refers to the thermal energy transportation by the rebounding particles. This mechanism has been analytically studied by Murray (1994a) for laminar thermal boundary layer in a cross flow over a tube wall. He found that the PRM is responsible for much of the measured heat transfer enhancement (Murray 1994b). For the problem under study, the PRM would be described as below; consider a typical small particle placed on the lower electrode and with temperature T_1 at time t_1 (It can be reasonably assumed that $T_1 \approx T_G$ where T_G refers to the grounded electrode temperature). The particle is moved upward by the Coulomb force and reaches the upper electrode at time t_2, having a temperature T_2. Depending on the particle velocity, size and material properties and the medium temperature distribution, T_2 will be lower than the surrounding liquid temperature, T_3 (It can reasonably assumed that $T_3 \approx T_{ue}$). Hence, the particle will absorb an amount of thermal energy from the surrounding liquid proportional to its residence time. The absorbed thermal energy will be released to the bulk of liquid while the particle travels downward. When the particle arrives to the lower electrode, it will release the left thermal energy to the liquid adjacent to the lower electrode during the particle residence time until it obtains the thermal equilibrium with the surrounding medium. This scenario will be repeated as the particle moves up and down inside the liquid.

For a given particle and working fluid, effectiveness of this mechanism, basically, depends on the particle velocity, the particle residence times near the electrodes and the temperature difference between the hot and cold surfaces. A suitable model and accurate calculations are needed to determine the functionality of this mechanism. However, it is worthy to pay more attention to this mechanism in the problem under study, which deals with the collision of electrically charged particles with an electrode at the presence of an electric field. Because as reported by Choi *et al.* (200), in this specific case, the charged particles, under some conditions, would settle on the electrode surface for a while. This settling time (or dwelling time (Capria, 2007)) is several times larger than a typical contact time. Opalinsky, (1988) has reported residence time of 0.2-1.5s caused by electrostatic effect in a typical fluidized bed. So, the so called particle residence time would be considerably large in this case which consequently would increase the role of this mechanism on the heat transfer from HTS to the adjacent liquid.

In addition to the convective heat transfer via BM, collision of particles with a HTS would cause the conduction of heat between the HTS and the colliding particles. Most of the available theories in this regard (Sun and Chen, 1988; Mei *et al.,* 2012) cannot be directly applied for the current study because they are based on the Hertzian contact theory (Johnson, 1987), which does not account for the repulsive and attractive electrical forces acting on the contacting bodies. According to the previous studies, often, the conductive heat transfer between the impinging particles and HTS is insignificant (Murray, 1994a; Li *et al.,* 2003). It is not thought that this mechanism can play important role in the current problem because of two reasons. Firstly, the wall hydrodynamic effect (Izard *et al.,* 2014) causes a considerable decrease in the impact velocity of particles which consequently reduces the contact area. Secondly, a thin layer of interstitial liquid prevents from direct contact between the approaching particles and the HTS. However, any probable enhancement from this mechanism can be easily included in the particle rebound mechanism (PRM) as described by Murray (1994b).

All of the above mentioned mechanisms originate from the motion of particles. In other words, those mechanisms cannot act without having moving particles inside the heat transfer medium. However, even stationary particles can alter the heat transfer rate by changing heat capacity of the medium. The determinant factor in this mechanism is $m_p c_p / m_f c_f = \varphi c_p / c_f$ which has been appeared in the Eq. (7). For the present experiments, magnitude of this term equals to 0.0022 and 0.0016 for silicon oil and opticool, respectively (see Table 1 for numerical values of the liquids' physical properties). Therefore, enhancement by this mechanism does not seem possible and it will not be considered as a relevant mechanism for the heat transfer enhancement observed in the current work.

8. RESULTS AND DISCUSSION

After introducing the relevant heat transfer enhancement mechanisms, we will now discuss the results of the tests. Figure 8 shows the results of the heat transfer enhancement (*HTEF*) with respect to the powered electrode voltage, *V*. The graph shows that *HTEF is* proportional to *V*, as expected from the increase of particle velocity with the magnitude of the applied electric field. It is also found that the enhancement for silicon oil is small in comparison with that for opticool liquid. Considering that the thermal conductivity of the two liquids are close, this difference must be due to the different velocity

of the particles, which arises from the large difference in dynamic viscosity of the two liquids. This result can be clearly seen in Fig. 9, that shows the data of Fig. 8 versus the averaged velocity of moving particles, $U = (u_{\infty 1} + u_{\infty 2})/2$. As seen in Figure 9, the results of experiments conducted with silicon oil and opticool liquid (tests of series A and B) show the same trend with respect to the moving particles velocity. In order to understand such behavior, we need to find out the role of particle velocity on the performance of the efficient mechanisms (BM, MM and PRM).

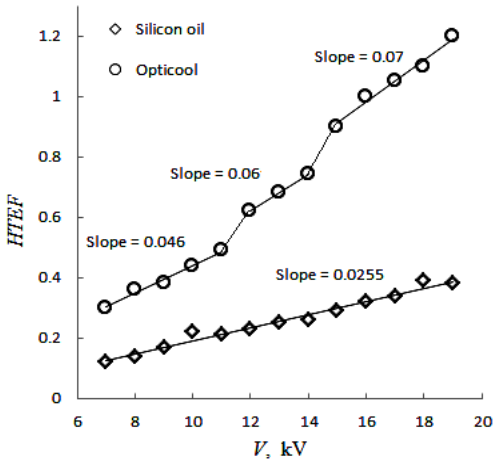

Fig. 8. Heat transfer enhancement for experiments done with 6000 ± 50 steel balls with $0.3 \pm 0.01mm$ diameter as solid conductive particles. Up and down motion of particles was kept for 5 minutes.

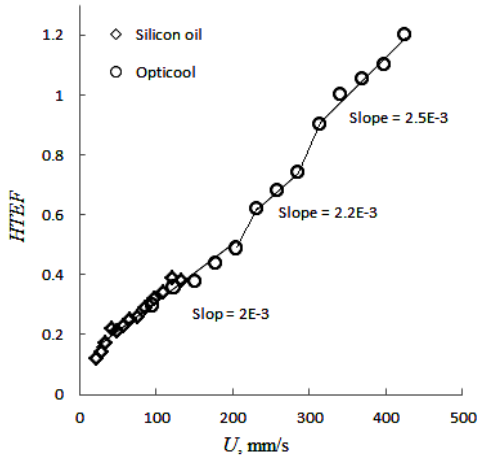

Fig. 9. Same as Fig. 8 but here the *HTEF* are plotted versus the mean velocity of conductive particles.

Basically, for a given interval (here 5 minutes), effectiveness of the BM on the heat transfer enhancement will improve with both the particle impinging velocity, u_{imp}, and the particle-electrode collision number, N_c. Since, both u_{imp} and N_c are proportional to U, it can be deduced that the BM performance will significantly improve with U. Considering MM, it is clear that the volume of displaced liquid caused by motion of a particle and the consequent mixing effect will be augmented with U. The PRM also is reinforced with increasing U because, as the particle velocity increases, larger amount of heat will be exchanged between the particle and the electrodes.

Therefore, it can be concluded that an increase in particles traveling velocity will intensify the three mechanisms. This is why the *HTEF* increases with U

Another remarkable feature of Fig. 9 is the sudden increment of *HTEF* for specific values of U, which is followed by an increase in the slope of data fitting lines (20% for the first jump and 18% for the second one). Also, this behavior can be observed in Fig. 8. The first and second jump in *HTEF* occurs when the powered electrode voltage increases from 11kV to 12 kV and from 14kV to 15kV, respectively (see Fig. 8). More information on the first and second jumps is given in Table 2.

Table 2 More information for cases involving the first and second sudden increment of *HTEF* (see Figs. 8 and 9)

	First jump			Second jump	
V, kV	11	12		14	15
$u_{\infty 1}$, m/s	152	183.4		245	275
$u_{\infty 2}$, m/s	256	280		329	354
$Re_{\infty 1}$	17	21		29	33
$Re_{\infty 2}$	28	34		39	42
HTEF	0.49	0.62		0.74	0.9

It is important to note that this phenomenon is not seen in the tests conducted with silicon oil. This unusual increase in *HTEF* cannot be attributed to the bombardment mechanism. As seen in Fig. 5, $Re_{\infty 1}$ and $Re_{\infty 2}$, and consequently $u_{\infty 1}$ and $u_{\infty 2}$, show almost a linear relation with the powered electrode voltage, V, in the tested range ($7kV \le V \le 18kV$), and no sudden increment is seen. We believe this phenomenon is related to the mixing mechanism. As mentioned previously, this mechanism depends on the particle diameter size and the wake structure behind the moving particle. Basically, the wake structure depends on the particle Reynolds number. Experimental investigation of Taneda (Brennen, 2005) demonstrated that at $Re \approx 30$, two rotating vortices are formed behind the sphere particle (see Fig. 10). We think these vortices significantly intensify the

mixing action in the liquid. Indeed, when a particle advances with $Re \geq 30$, two circulating zones survive in its path of motion due to rotational inertia of the vortices. The interaction among these circulating zones and moving particles enhances the mixing action in the bulk of the liquid. Interaction between detached vortices have been studied by Rehimi *et al.* (2010). Referring to Table 2, we see that for *V*=12kV the particle Reynolds number during the downward motion is *34* ($Re_{\infty 2} = 34$), which implies that the downward motion of particles is accompanied by rotating vortices. This is the main reason behind the first unusual increment of *HTEF* seen in the Figs. 8 and 9. This trend continues up to *V*=14kV. For the case *V*=15kV, both $Re_{\infty 1}$ and $Re_{\infty 2}$ are greater than 30 ($Re_{\infty 1} = 33$ and $Re_{\infty 2} = 43$). Therefore, in addition to the downward motion, the upward motion of particles also possesses such vortices. This causes stronger mixing in the liquid bulk which in turn brings about the second jump appearance observed in Figs. 9.

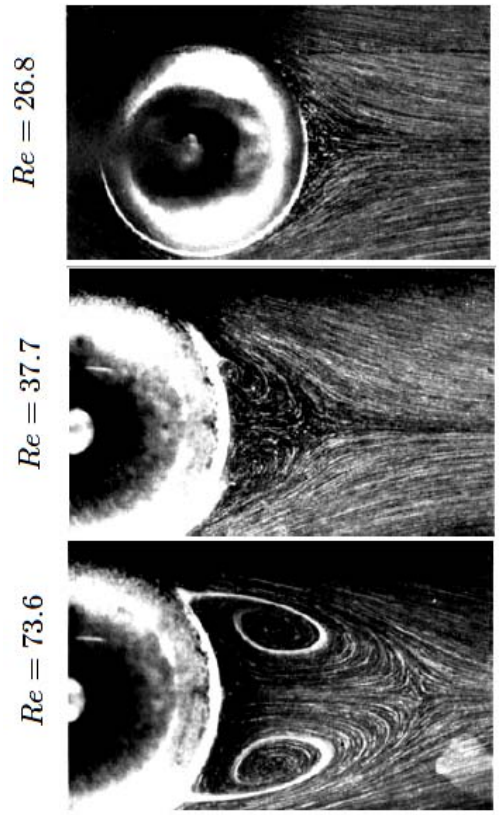

Fig. 10. Wake structure behind a sphere at various Reynolds numbers in the steady flow. Produced by Taneda (Brennen, 2005).

It is important to note that, in this investigation, the particles velocity has been calculated assuming a constant viscosity for the surrounding liquid. While, as it is known, the viscosity will reduce with increasing the liquid temperature. Therefore, the particles Reynolds number could have been underestimated here.

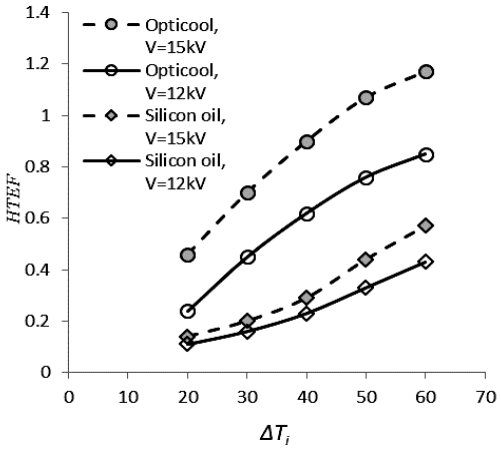

Fig. 11. Effect of the initial temperature difference between the upper electrode and the working fluid (ΔT_i) on the heat transfer enhancement factor (*HTEF*).

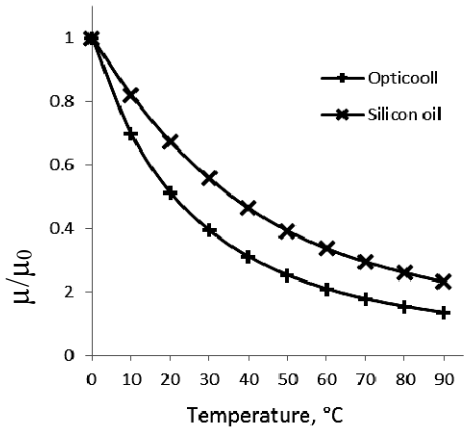

Fig. 12. Dimensionless viscosity of opticool and silicon oil at various temperatures. μ_0 stands for the dynamic viscosity at $T = 0$ °C and equals $0.0098 Pa.s$ and $0.0313 Pa.s$ for opticool and silicon oil, respectively.

Experimental results of series C are shown in Fig. 11. Irrespective of the working fluid and electric potential value, a remarkable increase in *HTEF* is observed with increasing initial temperature difference, ΔT_i. It seems that the dominant mechanisms (BM, MM and PRM) are intensified with ΔT_i. This improvement in *HTEF* can be attributed to the increase in the particles mean velocity *U*, which is caused by the reduction of the working fluid viscosity. For evaluating this idea, we measured viscosity of the working fluids in different temperatures. As the results show (depicted in Fig. 12), the dynamic viscosity of both opticool and silicon oil decreases significantly with the temperature. It is worth to note that the

Table 3 Details on the uncertainty of the instruments and parameters involved in the experiments

S. no	instrument	Working range	Measured variable	Least division in the instrument	Min. and Max. values measured in tests	Uncertainty, %
1	Thermocouple	(-20) - 150C°	T_{ue}	$0.1C^\circ$	$20.1\text{-}89C^\circ$	0.5975
2	Thermocouple	(-20) - 150C°	$T_{C,f}$	$0.1C^\circ$	$24.1\text{-}32.8C^\circ$	0.4149
3	Thermocouple	(-20) - 150C°	$T_{C,M}$	$0.1C^\circ$	$24.8\text{-}38.9C^\circ$	0.4032
4	Thermocouple	(-20) - 150C°	T_0	$0.1C^\circ$	$21\text{-}27C^\circ$	0.4762
5	Voltage	0 - 40kV	V	0.01kV	7 – 19kV	0.1429
6	Electric current	0 - 2.5mA	$I(t)$	10^{-12}A	3×10^{-9} – 1.5×10^{-6}A	0.0333
7	Number of particles		N_p		6000 ± 50	0.8333
8	Particle diameter		D		$300 \pm 5\mu m$	1.6666
9	Interelectrode gap		d		$20 \pm 0.2mm$	1
10	Liquid volume		V_{liquid}		0.1 ± 0.001 *litr*	1
11	Materials' properties	Density, thermal capacity, thermal conductivity,…				0.5

reduction of the viscosity can directly augment the particles Reynolds number in addition to the increasing of their velocity ($Re_\infty \propto u_\infty^1 \mu_f^{-1}$). Therefore, a more intense mixing mechanism (MM) is expected, which basically depends on the particle Reynolds number.

Increase in *HTEF* due to increasing the working fluid temperature - as observed in this study- is a special characteristic that could give an interesting self-controlling thermal property to a typical system which utilizes a flowing liquid as the heat transfer medium instead of a stagnant one. In fact, whenever the working fluid temperature increases due to insufficient heat transfer across the medium, its viscosity will decrease and consequently the *HTEF* will be augmented by the dominant mechanisms and will prevent the system from more warming.

9. CONCLUSION

In the present work, the heat transfer between a constant temperature plate and an adjacent stationary liquid was enhanced by means of spherical and sub-millimeter sized particles moving in the liquid medium. A uniform electric field was established between two parallel electrodes and utilized to excite and move the submerged conductive particles throughout the inter-electrode gap. It was experimentally demonstrated that such up and down motion of particles significantly enhances the heat transfer rate between a target electrode and the adjacent stationary liquid. Bombardment of the heat transfer surface by the moving particles (BM), the mixing action in the bulk of the base liquid that arises behind the moving particles (MM) and the thermal energy transported by the rebounding particles (PRM) were introduced as the effective mechanisms responsible for such enhancement. It was revealed that for the system under study, the particle velocity and its Reynolds number play an important role in the heat transfer enhancement mechanisms. It should be particularly noted that, although in the present study the Coulomb force was used for moving particles dispersed in liquid, the qualitative results, are valid if the particles are moved in a similar way by any other less hazardous agent such as magnetic forces.

APPNDIX

Uncertainty of the instruments and parameters involved in the current tests are given in Table 3. Uncertainty of HTEF is calculated as below;

$$HTEF = \eta - 1 \approx \left[1 + \varphi \frac{c_p}{c_f}\right] \frac{T_{C,M}(t) - T_0}{T_{C,f}(t) - T_0} - 1 \qquad (1A)$$
$$= F(T_0, T_{C,f}, T_{C,M}, \varphi, c_p, c_f),$$

The sensitivity coefficient of *HTEF* is (Beckwith *et al.*, 2007);

$$(\Delta HTEF)^2 = \left(\frac{\partial F}{\partial T_0}\Delta T_0\right)^2 + \left(\frac{\partial F}{\partial T_{C,f}}\Delta T_{C,f}\right)^2 +$$
$$\left(\frac{\partial F}{\partial T_{C,M}}\Delta T_{C,M}\right)^2 + \left(\frac{\partial F}{\partial \varphi}\Delta\varphi\right)^2 +$$

$$\left(\frac{\partial F}{\partial c_p}\Delta c_p\right)^2+\left(\frac{\partial F}{\partial c_f}\Delta c_f\right)^2. \tag{2A}$$

Considering Eqs. (1A) and (2A), the relative uncertainty of *HTEF* reads;

$$Un_{HTEF}=\frac{\Delta HTEF}{HTEF}\times 100\%. \tag{3A}$$

Irrespective of the accuracy of the proposed mathematical model in predicting the particles dynamics, there is some uncertainty in the averaged velocity of moving particles, $U=(u_{\infty 1}+u_{\infty 2})/2$ (U is depicted in horizontal axis of Fig. 9). This uncertainty comes from the measured parameters including the interelectrode gap (d), the particle diameter (D) and the powered electrode voltage (V). (see Eqs. (14) and (15). Note that $u_{\infty 1,2}=\mu Re_{\infty 1,2}/\rho_f D$). It is assumed that values of the physical properties of the materials (particles and liquids) are sufficiently accurate and don't bring about any significant error.

So the sensitivity coefficient of U reads;

$$(\Delta U)^2=\left(\frac{\partial U}{\partial d}\Delta d\right)^2+\left(\frac{\partial U}{\partial D}\Delta D\right)^2+\left(\frac{\partial U}{\partial V}\Delta V\right)^2 \tag{4A}$$

and,

$$Un_U=\frac{\Delta U}{U}\times 100\%. \tag{5A}$$

Equation (5A) can be used for calculating the relative uncertainty of U in each data point.

A simple program was set in MATLAB for calculating the derivatives appeared in Eqs. (3A) and (4A). Maximum values of 5.45% and 2.2% were obtained for Un_{HTEF} and Un_U, respectively

ACKNOWLEDGEMENT

The first author, Ghiyam Eslami wishes to express his deep appreciation to Antonio Ramos Reyes for providing him with facilities of the laboratory of Electrohydrodynamics in Seville university, Spain.

REFERENCES

Arcen, B., A. Taniere and M. Khalij (2012). Heat Transfer in a Turbulent Particle Laden Channel Flow. International Journal of Heat and Mass Transfer 55, 6519-6529.

Ardekani, A. and R. Rangel (2008). Numerical investigation of particle–particle and particle–wall collisions in a viscous fluid. *Journal of Fluid Mechanics* 596, 437-466.

Asano, K., C. R. Choi, K. Yatsuzuka and D. C. Lee (2002). Acceleration and deceleration of a conductive particle within parallel electrodes in viscous fluid. In*: Annual Report Conference on Electrical Insulation and Dielectric Phenomena, IEEE* 184-187.

Bacelos, M., C. Camargo, A. Silveira and J. Freire (2011). Local heat-transfer coefficient of immersed cylindrical surface in fluidized and vibrated fluidized beds. *Chemical Engineering and Processing: Process Intensification* 50, 1152-1159.

Beckwith, T. G., R. D. Marangoni and J. H. Lienhard (2007). Mechanical measurements. *Pearson Prentice Hall Upper Saddle River, NJ.*

Bologa, M. and A. Berkov (1987). Fluidization of electrically conductive particles in an electric force field. *Journal of Engineering Physics and Thermophysics* 53, 802-807.

Bologa, M., V. Pushkov and A. Berkov (1985). Electric field induced heat transfer enhancement in a gas-solid suspension heat exchanger. *International journal of heat and mass transfer* 28, 1245-1255.

Brennen, C. E. (2005). *Fundamentals of Multiphase Flow.* Cambridge University Press.

Capria, E. (2007). *Electrostatic manipulation of piezoelectric fibres using a sharp probe electrode in a dielectric liquid: Analysis of the electrohydrodynamic phenomena.* Ph. D. thesis, Cranfield University, London, England.

Choi, C., K. Yatsuzuka and K. Asano (2000). The behavior of spherical particle under uniform electric field in silicone oil. In: *Annual Report Conference on Electrical Insulation and Dielectric Phenomena, IEEE* 77-80.

Choi, C., K. Yatsuzuka and K. Asano (2001). Dynamic motion of a conductive particle in viscous fluid under DC electric field. *IEEE Transactions on Industry Applications* 37, 785-791.

Clift, R., J. Grace and M. Weber (1978). *Bubbles, Drops and Particles.* Academica Press, New York.

Dan, C. and A. Wachs (2010). Direct numerical simulation of particulate flow with heat transfer. *International Journal of Heat and Fluid Flow* 31, 1050-1057.

Dascalescu, L., M. Mihailescu and R. Tobazeon (1998). Modeling of conductive particle behavior in insulating fluids affected by DC electric fields. *IEEE Transactions on Industry Applications* 34, 66-74.

David, P. D., T. L. Bergman, A.S. Lavine and F.P. Incropera (2012). *Introduction to Heat Transfer.* Wiley, John and Sons.

Despeyroux, A. and A. Ambari (2012). Slow motion of a sphere towards a plane through confined non-Newtonian fluid. *Journal of Non-Newtonian Fluid Mechanics* 167, 38-45.

Drews, A. M., M. Kowalik and K. J. Bishop (2014). Charge and force on a conductive sphere between two parallel electrodes: A Stokesian

dynamics approach. *Journal of Applied Physics* 116(7).

Feng, Z. G. and E. E. Michaelides (2009). Heat transfer in particulate flows with direct numerical simulation (DNS). *International Journal of Heat and Mass Transfer* 52, 777-786.

Flamant, G., D. Gauthier, H. Benoit, J. L. Sans, B. Boissiere, R. Ansart and M. Hemati (2014). A new heat transfer fluid for concentrating solar systems: Particle flow in tubes. *Energy Procedia*. 49, 617-626.

Gan, H., J. Chang, J. J. Fen and H. H. Hu (2003). Direct numerical simulation of the sedimentation of solid particles with thermal convection. *Journal of Fluid Mechanics* 481, 385-411.

Hetsroni, G., M. Gurevich, R. Rozenblit, L. Yarin and G. Ziskind (2001). Effect of particle motion on the wall's thermal structure and on heat transfer. *International Journal of Multiphase Flow* 27, 393-413.

Izard, E., T. Bonometti and L. Lacaze (2014). Modelling the dynamics of a sphere approaching and bouncing on a wall in a viscous fluid. *Journal of Fluid Mechanics* 747, 422-446.

Johnson, K. L. (1987). *Contact Mechanics*. Cambridge Uiversity Press, London, England.

Kawamoto, H. (2009). Manipulation of single particles by utilizing electrostatic force. *Journal of Electrostatics* 67, 850-861.

Khaled, A. R. and K. Vafai (2004). Hydromagnetic squeezed flow and heat transfer over a sensor surface. *International Journal of Engineering Science* 42, 509-519.

Khaled, A. R. and K. Vafai (2005). Analysis of flow and heat transfer inside nonisothermal squeezed thin films. *Numerical Heat Transfer Part A: Applications* 47, 981-996.

Li, J., D. J. Mason and A. S. Mujumdar (2003). A numerical study of heat transfer mechanisms in gas–solids flows through pipes using a coupled CFD and DEM model. *Drying Technology* 21, 1839-1866..

Li, L., R. Mei, J. F. Klausner and D.W. Hah (2012). Heat transfer between colliding surfaces and particles, *Journal of Heat Transfer* 134(1).

Murray, D. (1994). Local enhancement of heat transfer in a particulate cross flow—I Heat transfer mechanisms. *International Journal of Multiphase Flow* 20, 493-504.

Murray, D. (1994b). Local enhancement of heat transfer in a particulate cross flow—II Experimental data and predicted trends. *International Journal of Multiphase Flow* 20, 505-513.

Nirmala G. S. and L. Muruganandam (2015). An Experimental Study of Liquid-Solid Flow in a Circulating Fluidized Bed of Varying Liquid Viscosity. *Journal of Applied Fluid Mechanics* 8(1), 95-101

Opaliński, I. and A. Wolny (1987). Discontinuity of particle contact with the surface and heat transfer in fluidized beds. *International journal of heat and mass transfer* 30, 589-599.

Özbelge, T. A. (2001). Heat transfer enhancement in turbulent upward flows of liquid–solid suspensions through vertical annuli. *International Journal of Heat and Mass Transfer* 44, 3373-3379.

Park, J. K., J. C. Ryu, W. K. Kim and K. H. Kan (2009). Effect of electric field on electrical conductivity of dielectric liquids mixed with polar additives: DC conductivity. *The Journal of Physical Chemistry B* 113(36), 12271-12276.

Pérez, A. T. (2002). Charge and force on a conducting sphere between two parallel electrodes. *Journal of Electrostatics* 56, 199-217.

Rawat, S., R. Bhargava, S. Kapoor, O. A. Bég, T. A. Bég and R. Bansal (2014). Numerical Modeling of Two-Phase Hydromagnetic Flow and Heat Transfer in a Particle-Suspension through a non-Darcian Porous Channel. *Journal of Applied Fluid Mechanics* 7(2), 249-261.

Rehimi, F., F. Aloui and S. B. Nasrallah (2011). Reorganization of coherent structures downstream a circular cylinder located between two parallel walls. *Journal of Applied Fluid Mechanics* 4(2), 51-56.

Schober, F., A. Küchler and C. Krause (2013). Oil conductivity–an important quantity for the design and the condition assessment of HVDC insulation systems. *FHWS Science Journal* 1(2), 59-78

Siebert, A., D. Highgate and M. Newborough (1999). Heat transfer characteristics of mechanically-stimulated particle beds. *Applied Thermal Engineering* 19, 37-49.

Sun, J. and M. Chen (1988). A theoretical analysis of heat transfer due to particle impact. *International Journal of Heat and Mass Transfer* 31, 969-975.

Wankhede, U., R. Sonolikar and S. Thombre (2011). Effect of acoustic field on heat transfer in a sound assisted fluidized bed of fine powders. *International Journal of Multiphase Flow* 37 1227-1234.

Xu, C., Y. Cheng and J. Zhu (2006). Fluidization of fine particles in a sound field and identification of group C/A particles using acoustic waves. *Powder Technology* 161, 227-234.

Zhebelev, S. (1991). Fluidization of microparticles in electric field. *Journal of Engineering physics* 60, 54-61.